Weierstraß-Institut
für Angewandte Analysis und Stochastik
Leibniz-Institut im Forschungsverbund Berlin e. V.

Preprint ISSN 0946 – 8633

Improving efficiency of coupled schemes for Navier-Stokes equations by a connection to grad-div stabilized projection methods

Alexander Linke[1], Michael Neilan[2], Leo G. Rebholz[3], Nicholas E. Wilson[4]

submitted: September 3, 2013

[1] Weierstrass Institute
Mohrenstr. 39
10117 Berlin, Germany
email: Alexander.Linke@wias-berlin.de

[2] University of Pittsburgh
Department of Mathematics
USA
email: neilan@pitt.edu

[3] Clemson University
Department of Mathematical Sciences
USA
email: rebholz@clemson.edu

[4] Michigan Tech
Department of Mathematical Sciences
Houghton, USA
email: newilson@mtu.edu

No. 1835
Berlin 2013

2010 *Mathematics Subject Classification.* 76D05, 65M60.

Key words and phrases. incompressible Navier-Stokes equations, projection method, grad-div stabilization, divergence-free finite element.

Edited by
Weierstraß-Institut für Angewandte Analysis und Stochastik (WIAS)
Leibniz-Institut im Forschungsverbund Berlin e. V.
Mohrenstraße 39
10117 Berlin
Germany

Fax: +49 30 20372-303
E-Mail: preprint@wias-berlin.de
World Wide Web: http://www.wias-berlin.de/

Abstract

We prove that in finite element settings where the divergence-free subspace of the velocity space has optimal approximation properties, the solution of Chorin/Temam projection methods for Navier-Stokes equations equipped with grad-div stabilization with parameter γ, converge to the associated coupled method solution with rate γ^{-1} as $\gamma \to \infty$. We prove this first for backward Euler schemes, and then extend the results to BDF2 schemes, and finally to schemes with outflow boundary conditions. Several numerical experiments are given which verify the convergence rate, and show how using projection methods in this setting with large grad-div stabilization parameters can dramatically improve accuracy.

1 Introduction

It is well known that solving velocity-pressure coupled linear systems that arise from numerical schemes for Navier-Stokes and related equations can be very challenging. Significant progress has been made in recent years (see e.g. [3, 8, 2] and references therein), but for many problems with higher Reynolds numbers or anisotropic meshes, it can be very difficult to find robust solvers.

To avoid this problem, scientists and engineers often use "Projection Methods", which were pioneered by Chorin and Teman [6, 23] in the 1960's. These methods decouple the system at each timestep, which changes the hard linear solve of a saddle point system into to easier linear solver, and an overall more efficient algorithm. Despite many improvement to projection methods since their development [12, 20, 19], they are still regarded in the CFD community as being less accurate (and less amenable to rigorous analytical study) than their coupled counterparts. The belief of less accuracy is based on lower pressure accuracy, a nonphysical pressure boundary condition $\nabla p \cdot \boldsymbol{n}|_{\partial\Omega} = 0$ is often enforced for efficiency purposes (so that a pressure Poisson problem can be solved instead of a saddle point problem), and a velocity solution is not found that is both incompressible and satisfies boundary conditions. Two velocity solutions are found with projection methods, one that satisfies the boundary conditions, and another that is divergence-free but only satisfies the normal component of the boundary conditions. Thus, the question arises, "which one should you use, if either?", since correct boundary prediction and mass conservation are both believed to be critical.

The purpose of this paper is show that, in some finite element settings, projection methods can be considered equivalent to coupled methods. We prove that, in finite element settings where the divergence-free subspace of the velocity space has optimal approximation properties, there is a strong connection between grad-div stabilized projection methods, and divergence-free coupled methods. More specifically, if we call the grad-div stabilization parameter γ, then as $\gamma \to \infty$, we prove that the boundary-condition-satisfying velocity solution and a modified pressure solution of the projection method converge to the coupled method's velocity and pressure solutions, with rate γ^{-1}. Thus, our results suggest that 'coupled-method-accuracy' can

be achieved with the projection method, if large grad-div stabilization parameters are used with appropriate meshes and approximating polynomial degrees. A significant amount of recent research has been done to determine when divergence-free subspaces of velocity spaces have optimal approximation properties (i.e., on what type meshes and with what polynomial degrees), and we review these results in section 2.

This paper is arranged as follows. In section 2, we present notation and some mathematical preliminaries to allow for a smooth analysis. We also discuss the specific requirements for the finite element setting where the connections are valid and give several examples. Section 3 proves the connection between the coupled backward Euler scheme and the backward Euler-type first order projection method. We also extend the results to the case of outflow boundary conditions and give numerical examples that verify the theory. In section 4, we extend these results to BDF2 schemes and provide additional numerical examples. Conclusions are given in section 5.

2 Mathematical preliminaries

We assume that the domain $\Omega \subset \mathbb{R}^d$ $(d = 2, 3)$ is open and connected with Lipschitz boundary $\partial\Omega$. For a positive integer m, we denote by $H^m(\Omega)$ the Hilbert space of $L^2(\Omega)$ functions whose distributional derivatives up to order m are in $L^2(\Omega)$. The space $H_0^m(\Omega)$ consists of $H^m(\Omega)$ functions with vanishing trace up to order $m-1$, and $L_0^2(\Omega)$ consists of square integrable functions with vanishing mean. The analogous vector-valued spaced are denoted in boldface; e.g., $\boldsymbol{H}^m(\Omega) := [H_0^m(\Omega)]^d$ and $\boldsymbol{H}_0^m(\Omega) := [H_0^m(\Omega)]^d$. The norm of $H^m(\Omega)$ is denoted by $\|\cdot\|_m$, and the $L^2(\Omega)$ norm and inner product are given by $\|\cdot\|$ and $(\cdot,\cdot)$, respectively. We further provide the shorthand notation

$$\begin{aligned} \boldsymbol{X} &:= \boldsymbol{H}_0^1(\Omega), & Q &:= L_0^2(\Omega), \\ \boldsymbol{V} &:= \{\boldsymbol{v} \in \boldsymbol{X}, \nabla\cdot\boldsymbol{v} = 0\}, & \boldsymbol{Y} &:= \{\boldsymbol{v} \in \boldsymbol{H}^1(\Omega), \boldsymbol{v}\cdot\boldsymbol{n}|_{\partial\Omega} = 0\}, \end{aligned}$$

where $\boldsymbol{n}$ denotes the outward unit normal of the boundary $\partial\Omega$. We define the skew-symmetric trilinear operator $b^* : \boldsymbol{X}\times\boldsymbol{X}\times\boldsymbol{X} \to \mathbb{R}$ by

$$b^*(\boldsymbol{u},\boldsymbol{v},\boldsymbol{w}) := \frac{1}{2}(\boldsymbol{u}\cdot\nabla\boldsymbol{v},\boldsymbol{w}) - \frac{1}{2}(\boldsymbol{u}\cdot\nabla\boldsymbol{w},\boldsymbol{v}).$$

Let $\mathcal{T}_h$ be a shape-regular, simplicial and conforming triangulation of Ω. Let $h_T = \mathrm{diam}(T)$ denote the diameter of a simplex T and define $h := \max_{T\in\mathcal{T}_h}$. We denote by $\mathcal{P}_k$ the space of piecewise polynomials with respect to the triangulation $\mathcal{T}_h$ with degree not exceeding k, and by $\boldsymbol{\mathcal{P}}_k := [\mathcal{P}_k]^d$ the analogous vector-valued polynomial space.

Throughout the paper, we consider finite dimensional spaces $\boldsymbol{X}_h,\ Q_h$ satisfying the following conditions.

Assumption 2.1. .

(i) Conforming*: The inclusions $\boldsymbol{X}_h \subset \boldsymbol{X}$ and $Q_h \subset Q$ hold;*

(ii) LBB stable*: The discrete inf-sup condition*

$$\inf_{q\in Q_h}\sup_{\boldsymbol{v}\in\boldsymbol{X}_h}\frac{(\nabla\cdot\boldsymbol{v},q)}{\|q\|\|\nabla\boldsymbol{v}\|} \geq \beta > 0 \tag{2.1}$$

is satisfied, where the constant β is independent of the discretization parameter h;

(iii) Exactly divergence-free*: The inclusion $\nabla\cdot\boldsymbol{X}_h \subseteq Q_h$ is satisfied;*

(iv) Approximation properties*: There exists $k \geq 1$ such that if $\boldsymbol{u} \in \boldsymbol{H}^k(\Omega)\cap\boldsymbol{X}$ and $p \in H^{k-1}(\Omega)\cap Q$, then*

$$\inf_{\boldsymbol{v}\in\boldsymbol{X}_h}\|\boldsymbol{u}-\boldsymbol{v}\|_1 \leq Ch^k\|\boldsymbol{u}\|_{k+1} \quad \textit{and} \quad \inf_{q\in Q_h}\|p-q\| \leq Ch^k\|p\|_k.$$

We further assume the existence of a finite element space $\boldsymbol{Y}_h \subset \boldsymbol{Y}$ with $\boldsymbol{X}_h \subset \boldsymbol{Y}_h$ and $\nabla \cdot \boldsymbol{Y}_h \subseteq Q_h$. Observe that the inf-sup condition (2.1) holds with $\boldsymbol{X}_h$ replaced by $\boldsymbol{Y}_h$.

We also define the space of discrete divergence-free functions

$$\boldsymbol{V}_h := \{\boldsymbol{v} \in \boldsymbol{X}_h : \ (\nabla \cdot \boldsymbol{v}, q) = 0 \ \forall q \in Q_h\}.$$

Due to assumption (iii), $\boldsymbol{V}_h$ is conforming to $\boldsymbol{V}$, i.e., functions in $\boldsymbol{V}_h \subset \boldsymbol{V}$ are divergence-free pointwise. We now list some finite element pairs that satisfy conditions (i)–(iv).

Examples 2.2.

(1) In [25, 1]*, it was shown that the choices* $\boldsymbol{X}_h = \boldsymbol{\mathcal{P}}_k \cap \boldsymbol{X}$ *and* $Q_h = \mathcal{P}_{k-1} \cap Q$ *with* $k \geq d$ $(d = 2, 3)$ *on a barycenter refinement of a triangular mesh satisfy the inf-sup condition* (2.1)*. Conditions (i), (iii), and (iv) are trivially satisfied due to the definitions of the spaces.*

(2) The Scott-Vogelius elements [22] $\boldsymbol{X}_h = \boldsymbol{\mathcal{P}}_k \cap \boldsymbol{X}$ *and* $Q_h = \mathcal{P}_{k-1} \cap Q$ *are known to fulfill conditions (i)–(iv) provided* (a) $d = 2$, (b) *the polynomial degree satisfies* $k \geq 4$*, and* (c) *the mesh does not contain any singular vertices, i.e., does not contain any vertices that lie on exactly two straight lines.*

(3) The finite element pairs constructed in [14] *satisfy the above conditions on general triangulations in two dimensions with* $k \geq 1$*. Here, the velocity space* $\boldsymbol{X}_h$ *consists of piecewise polynomials enriched locally with rational bubble functions and the pressure space* Q_h *consists of piecewise polynomials.*

(4) In [9]*, it was shown Hermite-type finite elements satisfy the conditions above in two dimensions provided each simplex does not have more than one boundary edge. In particular, the velocity space* $\boldsymbol{X}_h$ *consists of globally continuous piecewise polynomials of degree* $k \geq 4$ *that are* C^1 *at the vertices of the triangulation, and the pressure space* Q_h *consists of piecewise polynomials of degree* $k - 1$ *that are* C^0 *at vertices.*

Define $\boldsymbol{R}_h := \boldsymbol{V}_h^{\perp} \subset \boldsymbol{X}_h$ to be the complement of $\boldsymbol{V}_h$ with respect to the H^1 norm, i.e., $\boldsymbol{v} \in \boldsymbol{R}_h^{\perp}$ if $(\nabla \boldsymbol{v}, \nabla \boldsymbol{w}) = 0$ for all $\boldsymbol{w} \in \boldsymbol{X}_h$. The following lemma proves the divergence norm on $\boldsymbol{R}_h$ is equivalent to the gradient norm, with the constant C_R independent of h.

Lemma 2.1. *Let* $\boldsymbol{X}_h \times Q_h$ *satisfy the conforming property, the inf-sup condition and the divergence-free property given in Assumption 2.1, (i), (ii) (iii). We then have*

$$\|\nabla \boldsymbol{v}_h\| \leq C_R \|\nabla \cdot \boldsymbol{v}_h\| \qquad \forall \boldsymbol{v}_h \in \boldsymbol{R}_h, \tag{2.2}$$

where the constant C_R *is independent of* h*.*

Proof. Due to the inf-sup condition here exists a bounded projection $\boldsymbol{\Pi}_h : \boldsymbol{X} \to \boldsymbol{X}_h$ such that $(\nabla \cdot \boldsymbol{\Pi}_h \boldsymbol{v}_h, q_h) = (\nabla \cdot \boldsymbol{v}_h, q_h)$ and $\|\boldsymbol{\Pi}_h \boldsymbol{v}_h\|_1 \leq C \|\boldsymbol{v}_h\|_1$ for all $\boldsymbol{v}_h \in \boldsymbol{X}_h$ [5]. Let $\boldsymbol{v}_h \in \boldsymbol{R}_h$ be arbitrary, and set $0 \not\equiv q_h = \nabla \cdot \boldsymbol{v}_h$. Note $q_h \in Q_h$ due to assumption (iii). Let $\boldsymbol{w} \in \boldsymbol{X}$ satisfy $\nabla \cdot \boldsymbol{w} = q_h$ and $\|\boldsymbol{w}\|_1 \leq C \|q_h\|$ [10]. We then have

$$(\nabla \cdot (\boldsymbol{\Pi}_h \boldsymbol{w} - \boldsymbol{v}_h), r_h) = (\nabla \cdot (\boldsymbol{w} - \boldsymbol{v}_h), r_h) = 0 \qquad \forall r_h \in Q_h.$$

Since $\nabla \cdot \boldsymbol{V}_h \subseteq Q_h$, this implies $\boldsymbol{v}_h - \boldsymbol{\Pi}_h \boldsymbol{w} \in \boldsymbol{V}_h \cap \boldsymbol{R}_h = \{0\}$, i.e., $\boldsymbol{v}_h = \boldsymbol{\Pi}_h \boldsymbol{w}$. Consequently,

$$\|\boldsymbol{v}_h\|_1 = \|\boldsymbol{\Pi}_h \boldsymbol{w}\|_1 \leq C \|\boldsymbol{w}\|_1 \leq C \|q_h\| = C \|\nabla \cdot \boldsymbol{v}_h\|.$$

□

Remark 2.3. *If* $\boldsymbol{X}_h \times Q_h$ *satisfies (i) and if (iii) is replaced by* $\nabla \cdot \boldsymbol{V}_h = Q_h$*, then the inf-sup condition (ii) is equivalent to* (2.2)*. Indeed, if the inf-sup condition holds, then* (2.2) *is satisfied due to Lemma 2.1. On the other hand, suppose (i),* $\nabla \cdot \boldsymbol{V}_h = Q_h$*, and* (2.2)*. Let* $q \in Q_h$*, and let* $\boldsymbol{v}_h \in \boldsymbol{X}_h$ *satisfy* $\nabla \cdot \boldsymbol{v}_h = q_h$*. Then by* (2.2)*,* $\|\nabla \boldsymbol{v}_h\| \leq C_R \|q_h\|$ *and* (2.1) *easily follows.*

We will use the discrete Gronwall lemma in our convergence analysis in two forms. The first is the more common form, from [15].

Lemma 2.1 (Discrete Gronwall Lemma)**.** *Let Δt, H, and a_n, b_n, c_n, d_n (for integers $n \geq 0$) be nonnegative numbers such that*

$$a_\ell + \Delta t \sum_{n=0}^{\ell} b_n \leq \Delta t \sum_{n=0}^{\ell} d_n a_n + \Delta t \sum_{n=0}^{\ell} c_n + H \quad for\ \ell \geq 0.$$

If $\Delta t d_n < 1\ \forall n$, then

$$a_\ell + \Delta t \sum_{n=0}^{\ell} b_n \leq \exp\left(\Delta t \sum_{n=0}^{\ell} \frac{d_n}{1-\Delta t d_n}\right)\left(\Delta t \sum_{n=0}^{\ell} c_n + H\right) \quad for\ \ell \geq 0.$$

However, if $d_\ell = 0$, an improved Gronwall inequality is also remarked in [15] (page 370), which removes the dependence on Δt.

Lemma 2.2 (Alternative Discrete Gronwall Lemma)**.** *Let Δt, H, and a_n, b_n, c_n, d_n (for integers $n \geq 0$) be nonnegative numbers such that*

$$a_\ell + \Delta t \sum_{n=0}^{\ell} b_n \leq \Delta t \sum_{n=0}^{\ell-1} d_n a_n + \Delta t \sum_{n=0}^{\ell} c_n + H \quad for\ \ell \geq 1.$$

Then for $\Delta t > 0$,

$$a_\ell + \Delta t \sum_{n=0}^{\ell} b_n \leq \exp\left(\Delta t \sum_{n=0}^{\ell} d_n\right)\left(\Delta t \sum_{n=0}^{\ell} c_n + H\right) \quad for\ \ell \geq 1.$$

3 A connection for first order algorithms

We begin by recalling the linear extrapolated backward Euler timestepping with finite element discretization methods for the projection method [12, 20] and standard coupled method [17]. After stating the algorithms and known convergence results, we will prove that the grad-div stabilized projection scheme's solution converges to the coupled scheme's solution as the stabilization parameter $\gamma \to \infty$.

Algorithm 3.1 (BELEProjection)**.**
Let $\boldsymbol{f} \in \boldsymbol{L}^2(0,T;\boldsymbol{H}^{-1}(\Omega))$, solenoidal initial condition $\boldsymbol{u}^0 \in \boldsymbol{L}^2(\Omega)$ with $\boldsymbol{u}_h^0 = \widetilde{\boldsymbol{u}}_h^0$ defined to be the $\boldsymbol{L}^2$ projection of $\boldsymbol{u}^0$ into $\boldsymbol{V}_h$, stabilization parameter $\gamma > 0$, end time T, and timestep Δt be given. Set $M = T/\Delta t$, and for $n = 0, 1, 2, ..., M-1$,

Step 1: Find $\boldsymbol{u}_h^{n+1} \in \boldsymbol{X}_h$ satisfying, for all $\boldsymbol{\chi}_h \in \boldsymbol{X}_h$,

$$\frac{1}{\Delta t}(\boldsymbol{u}_h^{n+1} - \widetilde{\boldsymbol{u}}_h^n, \boldsymbol{\chi}_h) + b^*(\boldsymbol{u}_h^n, \boldsymbol{u}_h^{n+1}, \boldsymbol{\chi}_h) + \nu(\nabla \boldsymbol{u}_h^{n+1}, \nabla \boldsymbol{\chi}_h) + \gamma(\nabla \cdot \boldsymbol{u}_h^{n+1}, \nabla \cdot \boldsymbol{\chi}_h) = (\boldsymbol{f}(t^{n+1}), \boldsymbol{\chi}_h). \quad (3.1)$$

Step 2: Find $(\widetilde{\boldsymbol{u}}_h^{n+1}, p_h^{n+1}) \in (\boldsymbol{Y}_h, Q_h)$ satisfying, for all $(\boldsymbol{w}_h, q_h) \in (\boldsymbol{Y}_h, Q_h)$,

$$\frac{1}{\Delta t}(\widetilde{\boldsymbol{u}}_h^{n+1}, \boldsymbol{w}_h) - (p_h^{n+1}, \nabla \cdot \boldsymbol{w}_h) = \frac{1}{\Delta t}(\boldsymbol{u}_h^{n+1}, \boldsymbol{w}_h), \quad (3.2a)$$

$$(\nabla \cdot \widetilde{\boldsymbol{u}}_h^{n+1}, q_h) = 0. \quad (3.2b)$$

Note that $\boldsymbol{X}_h \subset \boldsymbol{Y}_h$, and therefore we can choose $\boldsymbol{w}_h = \boldsymbol{\chi}_h$ in (3.2) and plug into equation (3.1) to obtain

$$\frac{1}{\Delta t}(\boldsymbol{u}_h^{n+1} - \boldsymbol{u}_h^n, \boldsymbol{\chi}_h) - (p_h^n, \nabla \cdot \boldsymbol{\chi}_h) + b^*(\boldsymbol{u}_h^n, \boldsymbol{u}_h^{n+1}, \boldsymbol{\chi}_h)$$
$$+\nu(\nabla \boldsymbol{u}_h^{n+1}, \nabla \boldsymbol{\chi}_h) + \gamma(\nabla \cdot \boldsymbol{u}_h^{n+1} \nabla \cdot \boldsymbol{\chi}_h) = (\boldsymbol{f}(t^{n+1}), \boldsymbol{\chi}_h) \qquad \forall \boldsymbol{\chi}_h \in \boldsymbol{X}_h. \quad (3.3)$$

We note that typically the saddle point problem (3.2) is not solved as part of the projection method; instead a pressure-Poisson problem is solved with the boundary condition $\nabla p \cdot \boldsymbol{n}|_{\partial\Omega} = 0$ weakly enforced. However, when divergence-free finite elements are used, the iterated penalty method (see, e.g. [4]) can be used to efficiently solve the system. Also, this saddle point system is relatively easy to effectively precondition [8], and can also be solved with iterative methods. Hence, it is not unreasonable to require the saddle point system be solved instead of a pressure Poisson problem. Moreover, if the saddle point system is solved, the nonphysical boundary condition $\nabla p \cdot \boldsymbol{n}|_{\partial\Omega} = 0$ is not explicitly enforced.

Algorithm 3.2 (BELECoupled)**.** *Let $\boldsymbol{f} \in \boldsymbol{L}^2(0,T;\boldsymbol{H}^{-1}(\Omega))$, solenoidal initial condition $\boldsymbol{u}^0 \in \boldsymbol{L}^2(\Omega)$ with $\boldsymbol{v}_h^0$ defined to be the $\boldsymbol{L}^2$ projection of $\boldsymbol{u}^0$ into $\boldsymbol{V}_h$, end time T, and timestep Δt be given. Set $M = T/\Delta t$, and for $n = 1, 2, ..., M$, find $(\boldsymbol{v}_h^n, P_h^n) \in (\boldsymbol{X}_h, Q_h)$ satisfying*

$$\frac{1}{\Delta t}(\boldsymbol{v}_h^{n+1} - \boldsymbol{v}_h^n, \boldsymbol{\chi}_h) - (P_h^{n+1}, \nabla \cdot \boldsymbol{\chi}_h) + b^*(\boldsymbol{v}_h^n, \boldsymbol{v}_h^{n+1}, \boldsymbol{\chi}_h) \tag{3.4a}$$

$$+\nu(\nabla \boldsymbol{v}_h^{n+1}, \nabla \boldsymbol{\chi}_h) = (\boldsymbol{f}(t^{n+1}), \boldsymbol{\chi}_h) \qquad \forall \boldsymbol{\chi}_h \in \boldsymbol{X}_h,$$

$$(\nabla \cdot \boldsymbol{v}_h^{n+1}, q_h) = 0 \qquad \forall q_h \in Q_h. \tag{3.4b}$$

Both of the above algorithms are well-studied, and are known to admit unique solutions that converge as $\Delta t,\ h \to 0$ if the NSE solution is sufficiently smooth [19, 20, 13, 17]. Based on these results, we make the following assumptions about the boundedness of the schemes' solutions.

Assumption 3.3. *We assume that there exists a constant C_* which is independent of h, Δt, and γ, such that for sufficiently small h and Δt, solutions of Algorithms* 3.1 *and* 3.2 *satisfy*

$$\max_{1\le n\le M} (\|\nabla \boldsymbol{v}_h^n\| + \|\boldsymbol{v}_h^n\|_{L^\infty} + \|\nabla \boldsymbol{v}_h^n\|_{L^3}) \le C_*,$$

$$\max_{1\le n\le M} \|\nabla \boldsymbol{u}_h^n\| \le C_*.$$

Here, the constant $C_* > 0$ will depend on problem data, norms of the true solution, and potentially inverse inequality constants. If $\boldsymbol{u} \in \boldsymbol{L}^\infty(0,T;\boldsymbol{H}^3(\Omega))$, then there is no dependence on the inverse inequality constant.

3.1 Convergence of grad-div stabilized projection scheme velocity to coupled scheme velocity solution

We now prove that for a given sequence of grad-div stabilization parameters $\{\gamma_j\} \to \infty$, the corresponding sequence of solutions from Algorithm 3.1 will converge to the solution of Algorithm 3.2.

Theorem 3.4. *Given grad-div stabilization parameter γ, let $(\boldsymbol{v}_h^n, P_h^n)$ solve the BELECoupled system of Algorithm 3.2, and let $(\boldsymbol{u}_h^n, \widetilde{\boldsymbol{u}}_h^n, p_h^n)$ solve the BELEProj system of Algorithm 3.1, for $n = 1, 2, ..., M$. We then have*

$$\left(\Delta t \sum_{n=1}^{M} \|\nabla(\boldsymbol{u}_h^n - \boldsymbol{v}_h^n)\|^2\right)^{1/2} \le C\gamma^{-1}\nu^{-1/2} \max(\Delta t^{-1/2}, C_*\nu^{-1/2}) \left(\Delta t \sum_{n=0}^{M-1} \left(\left\|P_h^{n+1} - p_h^n\right\|^2\right)\right)^{1/2}, \tag{3.5}$$

and

$$\left(\Delta t \sum_{n=2}^{M-1} \left\|P_h^{n+1} - (p_h^n - \gamma \nabla \cdot \boldsymbol{u}_h^{n+1})\right\|^2\right)^{1/2}$$

$$\le C\gamma^{-1}\nu^{-1/2} \max(C_*\nu^{-1/2}, \Delta t^{-1/2}, C_*, \nu) \max(\Delta t^{-1/2}, C_*\nu^{-1/2}) \left(\Delta t \sum_{n=0}^{M-1} \left(\left\|P_h^{n+1} - p_h^n\right\|^2\right)\right)^{1/2}. \tag{3.6}$$

where $C > 0$ is independent of the timestep Δt, meshwidth h and stabilization parameter γ.

Remark 3.5. *On a fixed discretization, Theorem 3.4 proves first order convergence of grad-div stabilized BELEProj's boundary-condition-satisfying-velocity and modified pressure solutions to the BELECoupled velocity and pressure solutions, respectively, as* $\gamma \to \infty$.

Remark 3.6. *The estimates in Theorem 3.4 show a potential negative influence from a reduction of* Δt. *However, this negative influence should not typically be observed since the methods are known to converge, so we can expect* $\left(\Delta t \sum_{n=0}^{M-1} \left(\left\|P_h^{n+1} - p_h^n\right\|^2\right)\right)^{1/2}$ *to reduce this effect. Also, in practice, it is typically the case that* $C_*\nu^{-1/2} > \Delta t^{-1/2}$, *further removing the potential negative influence from shrinking* Δt.

Proof. Throughout this proof, C will represent a generic positive constant independent of h, γ, and Δt. Denote $\boldsymbol{e}^n := \boldsymbol{v}_h^n - \boldsymbol{u}_h^n$, and orthogonally decompose $\boldsymbol{e}^n$ by $\boldsymbol{e}^n = \boldsymbol{e}_0^n + \boldsymbol{e}_R^n$, where $\boldsymbol{e}_0^n \in \boldsymbol{V}_h$ and $\boldsymbol{e}_R^n \in \boldsymbol{R}_h$.
Step 1: Estimate of $\boldsymbol{e}_R^n$*:*
We begin by forming a difference equation by subtracting (3.3) from (3.4a) to get

$$\frac{1}{\Delta t}(\boldsymbol{e}^{n+1} - \boldsymbol{e}^n, \boldsymbol{\chi}_h) - (P_h^{n+1} - p_h^n, \nabla \cdot \boldsymbol{\chi}_h) + b^*(\boldsymbol{u}_h^n, \boldsymbol{e}^{n+1}, \boldsymbol{\chi}_h) + b^*(\boldsymbol{e}^n, \boldsymbol{v}_h^{n+1}, \boldsymbol{\chi}_h) + \nu(\nabla \boldsymbol{e}^{n+1}, \nabla \boldsymbol{\chi}_h) + \gamma(\nabla \cdot \boldsymbol{e}_R^{n+1}, \nabla \cdot \boldsymbol{\chi}_h) = 0 \quad \forall \boldsymbol{\chi}_h \in \boldsymbol{X}_h. \tag{3.7}$$

Choosing $\boldsymbol{\chi}_h = \boldsymbol{e}^{n+1}$, which vanishes the first nonlinear term, yields

$$\frac{1}{2\Delta t}\left(\|\boldsymbol{e}^{n+1}\|^2 - \|\boldsymbol{e}^n\|^2\right) + \nu\|\nabla \boldsymbol{e}^{n+1}\|^2 + \gamma\|\nabla \cdot \boldsymbol{e}_R^{n+1}\|^2 \leq (P_h^{n+1} - p_h^n, \nabla \cdot \boldsymbol{e}_R^{n+1}) - b^*(\boldsymbol{e}^n, \boldsymbol{v}_h^{n+1}, \boldsymbol{e}^{n+1}). \tag{3.8}$$

The right hand side terms of (3.8) are bounded above using the Cauchy-Schwarz and Young inequalities for the pressure term, and Holder's inequality, the Sobolev embedding theorem, Assumption 3.3, and Young's inequality for the nonlinear term:

$$\begin{aligned}
(P_h^n - p_h^n, \nabla \cdot \boldsymbol{e}_R^{n+1}) &\leq \frac{1}{2\gamma}\|P_h^{n+1} - p_h^n\|^2 + \frac{\gamma}{2}\|\nabla \cdot \boldsymbol{e}_R^{n+1}\|^2, \\
|b^*(\boldsymbol{e}^n, \boldsymbol{v}_h^{n+1}, \boldsymbol{e}^{n+1})| &\leq C\Big(\|\boldsymbol{e}^n\| \left\|\nabla \boldsymbol{v}_h^{n+1}\right\|_{L^3} \left\|\nabla \boldsymbol{e}^{n+1}\right\| + \|\boldsymbol{e}^n\| \left\|\boldsymbol{v}_h^{n+1}\right\|_{L^\infty} \left\|\nabla \boldsymbol{e}^{n+1}\right\| \Big) \\
&\leq CC_* \|\boldsymbol{e}^n\| \left\|\nabla \boldsymbol{e}^{n+1}\right\| \leq \frac{\nu}{2}\|\nabla \boldsymbol{e}^{n+1}\|^2 + CC_*^2\nu^{-1}\|\boldsymbol{e}^n\|^2.
\end{aligned}$$

Applying these estimates to (3.8) yields

$$\frac{1}{2\Delta t}\left(\|\boldsymbol{e}^{n+1}\|^2 - \|\boldsymbol{e}^n\|^2\right) + \frac{\nu}{2}\|\nabla \boldsymbol{e}^{n+1}\|^2 + \frac{\gamma}{2}\|\nabla \cdot \boldsymbol{e}_R^{n+1}\|^2 \leq CC_*^2\nu^{-1}\|\boldsymbol{e}^n\|^2 + \frac{1}{2\gamma}\|P_h^{n+1} - p_h^n\|^2.$$

Summing over time steps and applying Lemma 2.2 gives for all $\Delta t > 0$,

$$\|\boldsymbol{e}^M\|^2 + \Delta t \left(\sum_{n=0}^{M-1} \nu\|\nabla \boldsymbol{e}^{n+1}\|^2 + \gamma\|\nabla \cdot \boldsymbol{e}_R^{n+1}\|^2 \right) \leq C\gamma^{-1} \exp\left(C_*^2\nu^{-1}\right)) \, \Delta t \sum_{n=0}^{M-1} \|P_h^{n+1} - p_h^n\|^2.$$

Lemma 2.1 now provides us with

$$\Delta t \sum_{n=1}^{M} \|\nabla \boldsymbol{e}_R^n\|^2 \leq C_R \Delta t \sum_{n=1}^{M} \|\nabla \cdot \boldsymbol{e}_R^n\|^2 \leq C\gamma^{-2} \exp\left(C_*^2\nu^{-1}\right)) \left(\Delta t \sum_{n=0}^{M-1} \|P_h^{n+1} - p_h^n\|^2 \right). \tag{3.9}$$

Step 2: Estimate of $\boldsymbol{e}_0^n$*:*
It remains to bound $\Delta t \sum_{n=1}^{M} \|\nabla \boldsymbol{e}_0^n\|^2$ to complete the velocity estimate proof. To this end, we choose $\boldsymbol{\chi}_h = \boldsymbol{e}_0^{n+1}$ in (3.7) to obtain

$$\frac{1}{\Delta t}\left(\boldsymbol{e}^{n+1} - \boldsymbol{e}^n, \boldsymbol{e}_0^{n+1}\right) + \nu\|\nabla \boldsymbol{e}_0^{n+1}\|^2 = -b^*(\boldsymbol{e}^n, \boldsymbol{v}_h^{n+1}, \boldsymbol{e}_0^{n+1}) - b^*(\boldsymbol{u}_h^n, \boldsymbol{e}_R^{n+1}, \boldsymbol{e}_0^{n+1}). \tag{3.10}$$

Here, we have used the identity $b^*(\boldsymbol{u}_h^n, \boldsymbol{e}_0^{n+1}, \boldsymbol{e}_0^{n+1}) = 0$. The nonlinear terms are bounded using Holder's inequality, Assumption 3.3, and Young's inequality:

$$\begin{aligned} b^*(\boldsymbol{e}^n, \boldsymbol{v}_h^{n+1}, \boldsymbol{e}_0^{n+1}) &\leq CC_* \|\boldsymbol{e}^n\| \left\|\nabla \boldsymbol{e}_0^{n+1}\right\| \\ &\leq \frac{\nu}{4}\|\nabla \boldsymbol{e}_0^{n+1}\|^2 + CC_*^2\nu^{-1}\|\boldsymbol{e}^n\|^2, \end{aligned} \tag{3.11}$$

$$\begin{aligned} b^*(\boldsymbol{u}_h^n, \boldsymbol{e}_R^{n+1}, \boldsymbol{e}_0^{n+1}) &\leq C \|\nabla \boldsymbol{u}_h^n\| \left\|\nabla \boldsymbol{e}_R^{n+1}\right\| \left\|\nabla \boldsymbol{e}_0^{n+1}\right\| \\ &\leq CC_* \left\|\nabla \boldsymbol{e}_R^{n+1}\right\| \left\|\nabla \boldsymbol{e}_0^{n+1}\right\| \\ &\leq \frac{\nu}{2}\|\nabla \boldsymbol{e}_0^{n+1}\|^2 + CC_R C_*^2\nu^{-1}\|\nabla \cdot \boldsymbol{e}_R^{n+1}\|^2. \end{aligned} \tag{3.12}$$

The time derivative is bounded below by first adding and subtracting $\boldsymbol{e}_R^{n+1}$, using the polarization identity, and the Cauchy-Schwarz and Young's inequalities:

$$\begin{aligned} \frac{1}{\Delta t}\left(\boldsymbol{e}^{n+1} - \boldsymbol{e}^n, \boldsymbol{e}_0^{n+1}\right) &= \frac{1}{\Delta t}\left(\boldsymbol{e}^{n+1} - \boldsymbol{e}^n, \boldsymbol{e}^{n+1}\right) - \frac{1}{\Delta t}\left(\boldsymbol{e}^{n+1} - \boldsymbol{e}^n, \boldsymbol{e}_R^{n+1}\right) \\ &\geq \frac{1}{2\Delta t}\left(\left\|\boldsymbol{e}^{n+1}\right\|^2 - \|\boldsymbol{e}^n\|^2\right) + \frac{1}{2\Delta t}\left\|\boldsymbol{e}^{n+1} - \boldsymbol{e}^n\right\|^2 - \frac{1}{\Delta t}\left(\boldsymbol{e}^{n+1} - \boldsymbol{e}^n, \boldsymbol{e}_R^{n+1}\right) \\ &\geq \frac{1}{2\Delta t}\left(\left\|\boldsymbol{e}^{n+1}\right\|^2 - \|\boldsymbol{e}^n\|^2\right) - \frac{1}{2\Delta t}\left\|\boldsymbol{e}_R^{n+1}\right\|^2. \end{aligned} \tag{3.13}$$

Applying the estimates (3.11)–(3.13) and Lemma 2.1 to (3.10) gives us

$$\begin{aligned} \frac{1}{2\Delta t}\left(\|\boldsymbol{e}^{n+1}\|^2 - \|\boldsymbol{e}^n\|^2\right) + \frac{\nu}{4}\|\nabla \boldsymbol{e}_0^{n+1}\|^2 &\leq C\Big(C_*^2\nu^{-1}\|\boldsymbol{e}^n\|^2 + C_R C_*^2\nu^{-1}\|\nabla \cdot \boldsymbol{e}_R^{n+1}\|^2 + \frac{1}{\Delta t}\left\|\boldsymbol{e}_R^{n+1}\right\|^2\Big) \\ &\leq C\Big(C_*^2\nu^{-1}\|\boldsymbol{e}^n\|^2 + C_R(C_*^2\nu^{-1} + \Delta t^{-1})\|\nabla \cdot \boldsymbol{e}_R^{n+1}\|^2\Big). \end{aligned} \tag{3.14}$$

Multiplying by Δt on both sides, summing over timesteps produces

$$\left\|\boldsymbol{e}^M\right\|^2 + \nu\Delta t\sum_{n=1}^{M}\|\nabla \boldsymbol{e}_0^n\|^2 \leq C(C_*^2\nu^{-1} + \Delta t^{-1})\Delta t\sum_{n=1}^{M}\left\|\nabla \cdot \boldsymbol{e}_R^{n+1}\right\|^2 + \Delta t\left(\sum_{n=0}^{M-1} CC_*^2\nu^{-1}\left\|\boldsymbol{e}^n\right\|^2\right).$$

Now we apply Lemma 2.2 to get, for all $\Delta t > 0$,

$$\left\|\boldsymbol{e}^M\right\|^2 + \nu\Delta t\sum_{n=1}^{M}\|\nabla \boldsymbol{e}_0^n\|^2 \leq C\exp(C_*^2\nu^{-1})(C_*^2\nu^{-1} + \Delta t^{-1})\Delta t\sum_{n=1}^{M}\left\|\nabla \cdot \boldsymbol{e}_R^{n+1}\right\|^2.$$

Combining this estimate with (3.9) completes the proof for velocity.

Step 3: Pressure estimate:
For the pressure estimate, the difference equation (3.7) along with

$$\nabla \cdot \boldsymbol{e}_R^{n+1} = \nabla \cdot \boldsymbol{e}^{n+1} = \nabla \cdot (\boldsymbol{v}_h^{n+1} - \boldsymbol{u}_h^{n+1}) = \nabla \cdot \boldsymbol{u}_h^{n+1}.$$

provides the equation

$$(P_h^{n+1} - (p_h^n - \gamma\nabla \cdot \boldsymbol{u}_h^{n+1}), \nabla \cdot \boldsymbol{\chi}_h) = \frac{1}{\Delta t}(\boldsymbol{e}^{n+1} - \boldsymbol{e}^n, \boldsymbol{\chi}_h) + b^*(\boldsymbol{u}_h^n, \boldsymbol{e}^{n+1}, \boldsymbol{\chi}_h) + b^*(\boldsymbol{e}^n, \boldsymbol{v}_h^{n+1}, \boldsymbol{\chi}_h) + \nu(\nabla \boldsymbol{e}^{n+1}, \nabla \boldsymbol{\chi}_h).$$

Applying upper bounds similar to those above, using Assumption 3.3, dividing both sides by $\|\nabla \boldsymbol{\chi}_h\|$, and using the inf-sup condition yields

$$\beta_h\left\|P_h^{n+1} - (p_h^n - \gamma\nabla \cdot \boldsymbol{u}_h^{n+1})\right\| \leq C\left(\frac{1}{\Delta t}\left\|\boldsymbol{e}^{n+1} - \boldsymbol{e}^n\right\| + (C_* + \nu)\left\|\nabla \boldsymbol{e}^{n+1}\right\| + C_*\left\|\nabla \boldsymbol{e}^n\right\|\right). \tag{3.15}$$

Thus, using (3.14) and reducing gives

$$\begin{aligned}
&\left\|P_h^{n+1} - (p_h^n - \gamma\nabla\cdot\boldsymbol{u}_h^{n+1})\right\|^2 \\
&\leq \quad C\left(\left(C_*^2\nu^{-1} + \frac{1}{2\Delta t}\right)\|\boldsymbol{e}^n\|^2 + (C_*^2\nu^{-1} + \Delta t^{-1})\|\nabla\cdot\boldsymbol{e}_R^{n+1}\|^2 + (C_*^2+\nu^2)\left\|\nabla\boldsymbol{e}^{n+1}\right\|^2 + C_*^2\left\|\nabla\boldsymbol{e}^n\right\|^2\right) \\
&\leq \quad C\left(\left(C_*^2\nu^{-1} + \Delta t^{-1} + C_*^2\right)\|\nabla\boldsymbol{e}^n\|^2 + (C_*^2\nu^{-1} + \Delta t^{-1} + C_*^2 + \nu^2)\left\|\nabla\boldsymbol{e}^{n+1}\right\|^2\right). \qquad (3.16)
\end{aligned}$$

Multiplying by Δt, summing over timesteps and reducing produces the bound

$$\Delta t\sum_{n=1}^{M-1}\left\|P_h^{n+1} - (p_h^n - \gamma\nabla\cdot\boldsymbol{u}_h^{n+1})\right\|^2 \leq C\left(C_*^2\nu^{-1} + \Delta t^{-1} + C_*^2 + \nu^2\right)\Delta t\sum_{n=1}^{M-1}\left\|\nabla\boldsymbol{e}^{n+1}\right\|^2. \qquad (3.17)$$

Combining this with the velocity estimate completes the proof.

□

3.2 Outflow boundary conditions

We consider now the important physical case of a boundary that includes outflow boundary conditions, i.e. $\partial\Omega = \Gamma_1\cup\Gamma_2$, with velocity boundary conditions $\boldsymbol{u}|_{\Gamma_1} = \boldsymbol{0}$ and $(-\nu\nabla\boldsymbol{u}+pI)\cdot\boldsymbol{n}|_{\Gamma_2} = \boldsymbol{0}$. We could equivalently consider the deformation tensor form of the natural boundary condition, by using the deformation tensor in the variational formulation; this outflow condition is commonly referred to as 'zero traction'. For simplicity, we consider just the gradient form.

For coupled schemes, the natural boundary condition is usually implemented as a 'do-nothing' condition at the outflow, i.e. by simply dropping the resulting boundary integral from the variational formulation. For example, if we change the definition of the velocity space so that

$$\boldsymbol{X}_h = \{\boldsymbol{v}_h \in \boldsymbol{\mathcal{P}}_k(\mathcal{T}_h)\cap\boldsymbol{H}^1(\Omega),\ \boldsymbol{v}_h|_{\Gamma_1} = \boldsymbol{0}\}, \qquad (3.18)$$

then the BELECoupled algorithm of Algorithm 3.2 will weakly enforce the outflow boundary condition $\left((-\nu\nabla\boldsymbol{u}_h^{n+1} + p_h^{n+1}I)\cdot\boldsymbol{n}\right)|_{\Gamma_2} = \boldsymbol{0}$.

The situation is somewhat different for BELEProjection, since the boundary integrals for velocity and pressure appear in different steps. The definition of $\boldsymbol{X}_h$ (3.18) will be used, and the natural boundary condition $\left((-\nu\nabla\boldsymbol{u}_h^{n+1} - \gamma(\nabla\cdot\boldsymbol{u}_h^{n+1})I)\cdot\boldsymbol{n}\right)|_{\Gamma_2} = \boldsymbol{0}$ will be implemented in step 1 by dropping the resulting boundary integral in the variational formulation. In step 2, we also implement the Dirichlet condition $p_h^{n+1}|_{\Gamma_2} = 0$, and change the definition of this velocity space to

$$\boldsymbol{Y}_h = \{\boldsymbol{v}_h \in \boldsymbol{\mathcal{P}}_k(\mathcal{T}_h)\cap\boldsymbol{H}^1(\Omega),\ \boldsymbol{v}_h\cdot\boldsymbol{n}|_{\Gamma_1} = 0\}. \qquad (3.19)$$

With these definitions for $\boldsymbol{X}_h$ and $\boldsymbol{Y}_h$, and the enforcement of the projection method pressure to be zero on Γ_2, the schemes can be analyzed in the exact same way as in Algorithms 3.1 and 3.2. Thus we have the following result:

Theorem 3.7. *Replace in Algorithm 3.2 (BELECoupled) and Algorithm 3.1 (BELEProj) the definition of $\boldsymbol{X}_h$ from (3.18) and $\boldsymbol{Y}_h$ from (3.19), using that $\partial\Omega = \Gamma_1\cup\Gamma_2$. Then given grad-div stabilization parameter γ, let $(\boldsymbol{v}_h^n, P_h^n)$ solve BELECoupled, and let $(\boldsymbol{u}_h^n, \widetilde{\boldsymbol{u}}_h^n, p_h^n)$ solve BELEProj, for $n = 1, 2, ..., M$. We then have*

$$\left(\Delta t\sum_{n=1}^{M}\|\nabla(\boldsymbol{u}_h^n - \boldsymbol{v}_h^n)\|^2\right)^{1/2} \leq C\gamma^{-1}\nu^{-1/2}\max(\Delta t^{-1/2}, C_*\nu^{-1/2})\left(\Delta t\sum_{n=0}^{M-1}\left(\left\|P_h^{n+1} - p_h^n\right\|^2\right)\right)^{1/2}, \qquad (3.20)$$

and

$$\left(\Delta t \sum_{n=2}^{M-1} \left\| P_h^{n+1} - (p_h^n - \gamma \nabla \cdot \boldsymbol{u}_h^{n+1}) \right\|^2 \right)^{1/2}$$

$$\leq C\gamma^{-1}\nu^{-1/2} \max(C_*\nu^{-1/2}, \Delta t^{-1/2}, C_*, \nu) \max(\Delta t^{-1/2}, C_*\nu^{-1/2}) \left(\Delta t \sum_{n=0}^{M-1} \left(\left\| P_h^{n+1} - p_h^n \right\|^2 \right) \right)^{1/2}, \quad (3.21)$$

where $C > 0$ is independent of the timestep Δt, meshwidth h and stabilization parameter γ.

Remark 3.8. *Similar to the full Dirichlet boundary case presented in Theorem 3.5, we do not generally expect a negative influence from Δt in practice (cf. Remark 3.6).*

Remark 3.9. *By writing the modified pressure $\widetilde{p}_h^{n+1} = p_h^n - \gamma(\nabla \cdot \boldsymbol{u}_h^{n+1})$, and using the boundary condition $p_h^{n+1}|_{\Gamma_2} = 0$, the natural boundary condition for the projection method can be written as*

$$\int_{\Gamma_2} \left((-\nu \nabla \boldsymbol{u}_h^{n+1} - \gamma(\nabla \cdot \boldsymbol{u}_h^{n+1}) I) \cdot \boldsymbol{n} \right) \cdot \boldsymbol{\chi}_h \, ds = \int_{\Gamma_2} \left((-\nu \nabla \boldsymbol{u}_h^{n+1} - \widetilde{p}_h^{n+1} I) \cdot \boldsymbol{n} \right) \cdot \boldsymbol{\chi}_h \, ds.$$

Thus by Theorem 3.7, this outflow condition converges to the outflow condition for the coupled system as $\gamma \to 0$ for a fixed discretization.

3.3 Numerical experiments for the first order schemes

We now numerically test the results of Theorem 3.4 by comparing solutions from Algorithm 3.1 with varying γ to the solution of Algorithm 3.2, in the norms of Theorem 3.4:

$$\|\phi\|_{2,1} := \left(\Delta t \sum_{n=1}^{M} \|\nabla \phi^n\|^2 \right)^{1/2}, \quad \|\phi\|_{2,0} := \left(\Delta t \sum_{n=2}^{M} \|\phi^n\|^2 \right)^{1/2}.$$

3.3.1 Channel flow past a forward-backward step with Dirichlet boundary conditions

We first test the theory on the benchmark two dimensional problem of channel flow past a forward-backward facing step. The domain is a 40×10 rectangle, with a 1×1 step placed five units into the channel at the bottom. No slip boundary conditions are enforced on all walls, and a parabolic inflow and outflow conditions are given by $(y(10-y)/25, 0)^T$. The correct physical behavior with $\boldsymbol{f} = \boldsymbol{0}$ and $\nu = 1/600$ is a smooth velocity profile, with eddies forming and detaching behind the step [18].

We take $\boldsymbol{X}_h = \boldsymbol{\mathcal{P}}_k \cap \boldsymbol{X}$ and $Q_h = \mathcal{P}_{k-1} \cap Q$ on a baycenter refined triangular mesh (cf. Examples 2.2). We choose $k = 2$, $T = 40$, $\Delta t = 0.1$ (M=400), and compute the solution on a barycenter refined triangular mesh, which provides 11,774 total degrees of freedom (dof) for the velocity space $\boldsymbol{X}_h$, and 8,658 dof for Q_h. We note that this mesh is not quite sufficiently fine to fully resolve the flow; we do this intentionally in order to observe the differences between the two algorithms.

The differences between the projection method solutions with varying γ and the coupled scheme solution are reported in Table 1. We observe results that are consistent with first order convergence for both velocity and pressure.

We also display plots of the solutions' velocity streamlines over speed contours as well as pressure contours in Figure 1 for the projection method, and Figure 2 for the coupled method. The coupled method velocity solution agrees with the known resolved solution from [18], while the projection method solution with $\gamma = 0$ does not accurately predict the eddies behind the step. As γ increases, the convergence to the coupled system solution is clear from the plots, and by γ =10,000 the coupled solution and grad-div stabilized projection solution are indistinguishable.

γ	$\|\boldsymbol{u}_{h,\gamma} - \boldsymbol{v}_h\|_{2,1}$	rate	$\|\hat{p}_h - P_h\|_{2,0}$	rate
0	6.976e-0	-	4.295e-1	-
1	3.901e-0	0.252	3.580e-1	0.079
10	1.812e-0	0.333	2.017e-1	0.249
100	4.556e-1	0.600	6.313e-2	0.505
1,000	6.306e-2	0.859	1.153e-2	0.738
10,000	6.889e-3	0.962	1.203e-3	0.982

Table 1: Differences between projection method and coupled system solutions with varying γ for the flow over a step test problem. In the table, $\hat{p}_h^n = p_h^{n-1} - \gamma \nabla \cdot \boldsymbol{u}_h^n$. The results are consistent with first order convergence for both velocity and modified pressure.

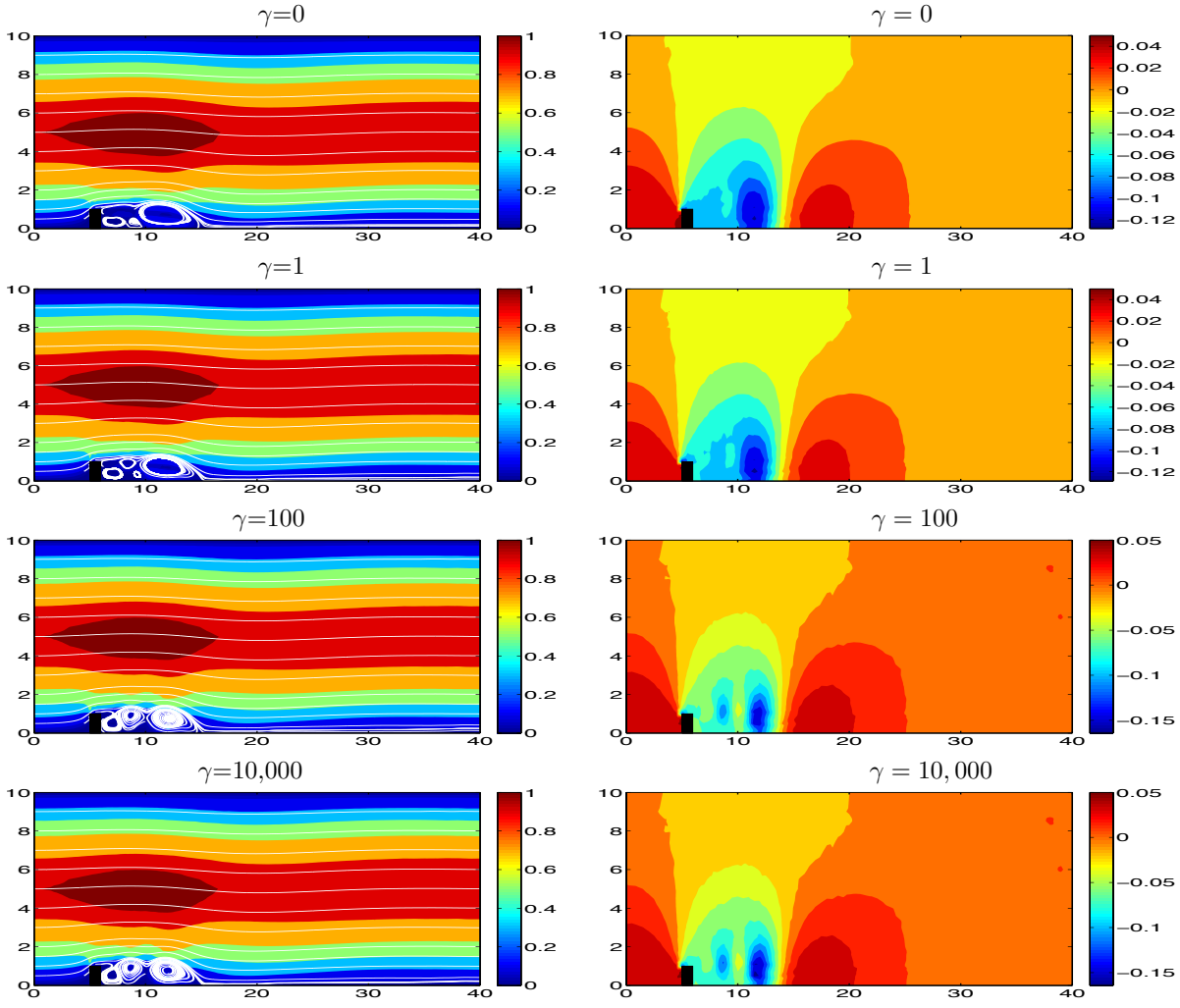

Figure 1: Shown above is solution of Algorithm 3.1 at $T = 40$ with varying γ, with velocity streamlines over speed contours on the left, and a contour plot of the modified pressure on the right.

3.3.2 Channel flow past a forward-backward step with outflow boundary conditions

We now repeat the channel flow over a step experiment, but with the outflow boundary condition $(-\nu\nabla\boldsymbol{u} - pI)\cdot\boldsymbol{n} = \boldsymbol{0}$ enforced as discussed in section 3.2; that is, as a natural boundary condition for BELECoupled,

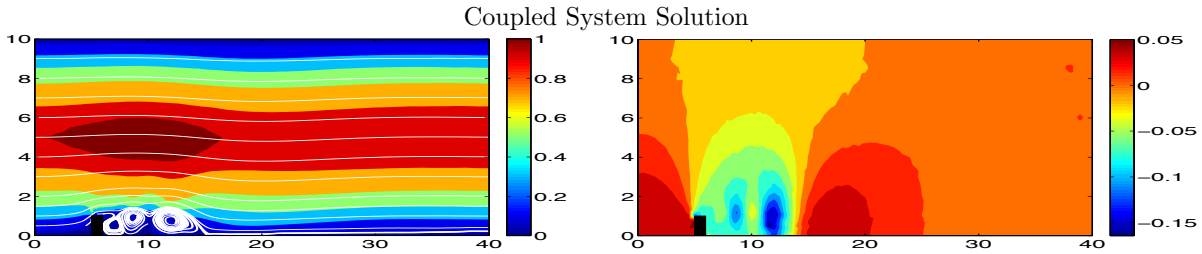

Figure 2: Shown above is the velocity (left) and pressure (right) solution of Algorithm 3.2 at $T = 40$.

and as a natural boundary condition in step 1 of BELEProj, but enforcing the pressure to be zero at the outflow in step 2 of BELEProj. All other parameters are the same as in the tests for full Dirichlet boundary conditions.

Table 2 shows the difference between the velocity and pressure solutions of the projection and coupled methods for varying γ. We observe very similar results as in the case of full Dirichlet boundary conditions for velocity, but slightly different for pressure. Although it appears the pressure rate will increase to one, by $\gamma = 10,000$ it is not as close as in the case of full Dirichlet boundary conditions. The velocity does appear to have first order convergence. The plots of the solutions are nearly identical to those with full Dirichlet boundary conditions, and so they are omitted.

γ	$\|\boldsymbol{u}_{h,\gamma} - \boldsymbol{v}_h\|_{2,1}$	rate	$\|\hat{p}_h - P_h\|_{2,0}$	rate
0	6.971e-0	-	4.292e-1	-
1	3.898e-0	0.252	3.587e-1	0.078
10	1.811e-0	0.333	2.031e-1	0.247
100	4.556e-1	0.600	6.465e-2	0.497
1,000	6.307e-2	0.859	1.661e-2	0.590
10,000	7.083e-3	0.950	3.508e-3	0.675

Table 2: Differences between projection method and coupled system solutions with varying γ, for the flow over a step test problem using outflow boundary conditions. In the table, $\hat{p}_h^n = p_h^{n-1} - \gamma \nabla \cdot \boldsymbol{u}_h^n$. The results are consistent with a convergence rate of 1 for both velocity and modified pressure.

4 A connection for second order algorithms

We begin by recalling the linear extrapolated BDF2 timestepping with finite element discretization methods for the projection method [12] and standard coupled method [17]. We assume a given $\boldsymbol{f} \in \boldsymbol{L}^2(0,T;\boldsymbol{H}^{-1}(\Omega))$, solenoidal initial conditions $\boldsymbol{u}^1,\ \boldsymbol{u}^0 \in \boldsymbol{L}^2(\Omega)$ with $\boldsymbol{v}_h^1 = \boldsymbol{u}_h^1$ and $\boldsymbol{v}_h^0 = \boldsymbol{u}_h^0$ defined to be the L^2 projections of the initial conditions into $\boldsymbol{V}_h$. After stating the algorithms and their known convergence results, we will prove that the grad-div stabilized projection scheme solutions converge to the coupled scheme solution as the stabilization parameter $\gamma \to \infty$.

Algorithm 4.1 (BDF2Proj)**.**
Step 1: Find $\boldsymbol{u}_h^{n+1} \in \boldsymbol{X}_h$ *satisfying, for all* $\boldsymbol{\chi}_h \in \boldsymbol{X}_h$,

$$\frac{1}{2\Delta t}(3\boldsymbol{u}_h^{n+1} - 4\widetilde{\boldsymbol{u}_h^n} + \widetilde{\boldsymbol{u}_h^{n-1}}, \boldsymbol{\chi}_h) + b^*(2\boldsymbol{u}_h^n - \boldsymbol{u}_h^{n-1}, \boldsymbol{u}_h^{n+1}, \boldsymbol{\chi}_h) \tag{4.1}$$
$$+\nu(\nabla \boldsymbol{u}_h^{n+1}, \nabla \boldsymbol{\chi}_h) - (p_h^n, \nabla \cdot \boldsymbol{\chi}_h) + \gamma(\nabla \cdot \boldsymbol{u}_h^{n+1}, \nabla \cdot \boldsymbol{\chi}_h) = (\boldsymbol{f}(t^{n+1}), \boldsymbol{\chi}_h).$$

Step 2: Find $(\widetilde{\boldsymbol{u}}_h^{n+1}, p_h^{n+1}) \in (\boldsymbol{Y}_h, Q_h)$ *satisfying, for all* $(\boldsymbol{w}_h, q_h) \in (\boldsymbol{Y}_h, Q_h)$,

$$\frac{3}{2\Delta t}(\widetilde{\boldsymbol{u}}_h^{n+1} - \boldsymbol{u}_h^{n+1}, w_h) - (p_h^{n+1} - p_h^n, \nabla \cdot w_h) = 0, \tag{4.2a}$$

$$(\nabla \cdot \widetilde{\boldsymbol{u}}_h^{n+1}, q_h) = 0. \tag{4.2b}$$

Similar to the first order schemes, we can choose $\boldsymbol{w}_h = \boldsymbol{\chi}_h$ in (4.2), and plug into (4.1) to reveal that $\boldsymbol{u}_h^{n+1} \in \boldsymbol{X}_h$ satisfies $\forall \boldsymbol{\chi}_h \in \boldsymbol{X}_h$,

$$\begin{aligned} &\frac{1}{2\Delta t}(3\boldsymbol{u}_h^{n+1} - 4\boldsymbol{u}_h^n + \boldsymbol{u}_h^{n-1}, \boldsymbol{\chi}_h) - \left(\frac{7}{3}p_h^n - \frac{5}{3}p_h^{n-1} + \frac{1}{3}p_h^{n-2}, \nabla \cdot \boldsymbol{\chi}_h\right) \\ &+b^*(2\boldsymbol{u}_h^n - \boldsymbol{u}_h^{n-1}, \boldsymbol{u}_h^{n+1}, \boldsymbol{\chi}_h) + \nu(\nabla \boldsymbol{u}_h^{n+1}, \nabla \boldsymbol{\chi}_h) + \gamma(\nabla \cdot \boldsymbol{u}_h^{n+1}, \nabla \cdot \boldsymbol{\chi}_h) = (\boldsymbol{f}(t^{n+1}), \boldsymbol{\chi}_h). \end{aligned} \tag{4.3}$$

We note that the pressure term can be considered a second order extrapolation approximation to p_h^{n+1}.

Algorithm 4.2 (BDF2Coupled)**.** *Find* $(\boldsymbol{v}_h^{n+1}, P_h^{n+1}) \in \boldsymbol{X}_h \times Q_h$ *satisfying*

$$\begin{aligned} &\frac{1}{2\Delta t}(3\boldsymbol{v}_h^{n+1} - 4\boldsymbol{v}_h^n + \boldsymbol{v}_h^{n-1}, \boldsymbol{\chi}_h) - (P_h^{n+1}, \nabla \cdot \boldsymbol{\chi}_h) && \text{(4.4a)} \\ &\quad +b^*(2\boldsymbol{v}_h^n - \boldsymbol{v}_h^{n-1}, \boldsymbol{v}_h^{n+1}, \boldsymbol{\chi}_h) + \nu(\nabla \boldsymbol{v}_h^{n+1}, \nabla \boldsymbol{\chi}_h) = (\boldsymbol{f}(t^{n+1}), \boldsymbol{\chi}_h) \qquad \forall \boldsymbol{\chi}_h \in \boldsymbol{X}_h, \\ &\qquad (\nabla \cdot \boldsymbol{v}_h^{n+1}, q_h) = 0 \qquad \forall q_h \in Q_h. && \text{(4.4b)} \end{aligned}$$

Based on known convergence result for these methods [11, 13, 12, 17], we make the following assumptions about the boundedness of the schemes' solutions.

Assumption 4.3. *We assume that there exists a constant* C_* *which is independent of* h, Δt, *and* γ, *such that for sufficiently small* h *and* Δt, *solutions of Algorithms* 4.1 *and* 4.2 *satisfy*

$$\max_{1 \le n \le M} (\|\nabla \boldsymbol{v}_h^n\| + \|\boldsymbol{v}_h^n\|_{L^\infty} + \|\nabla \boldsymbol{v}_h^n\|_{L^3}) \le C_*,$$

$$\max_{1 \le n \le M} \|\nabla \boldsymbol{u}_h^n\| \le C_*.$$

Here, the constant $C_* > 0$ *will depend on problem data, norms of the true solution, and potentially inverse inequality constants. If* $\boldsymbol{u} \in \boldsymbol{L}^\infty(0, T; \boldsymbol{H}^3(\Omega))$, *then there is no dependence on the inverse inequality constant.*

4.1 Convergence of BDF2 grad-div stabilized projection scheme solution to coupled BDF2 scheme solution

Theorem 4.4. *Given grad-div stabilization parameter* γ, *let* $(\boldsymbol{v}_h^n, P_h^n)$ *solve the BDF2Coupled system of Algorithm 4.2, and let* $(\boldsymbol{u}_h^n, \widetilde{\boldsymbol{u}}_h^n, p_h^n)$ *solve the BDF2Proj system of Algorithm 4.1, for* $n = 1, 2, ..., M$. *Denote*

$$C_P := \left(\Delta t \sum_{n=2}^{M-1} \left\| P_h^{n+1} - \left(\frac{7}{3}p_h^n - \frac{5}{3}p_h^{n-1} + \frac{1}{3}p_h^{n-2}\right)\right\|^2\right)^{1/2}.$$

For $\Delta t < 1$, *we have*

$$\left(\Delta t \sum_{n=1}^{M} \|\nabla(\boldsymbol{u}_h^n - \boldsymbol{v}_h^n)\|^2\right)^{1/2} \le C\nu^{-1/2} C_P^{1/2} \gamma^{-1} \max(\Delta t^{-1}, C_* \nu^{-1/2}), \tag{4.5}$$

and

$$\begin{aligned} &\left(\Delta t \sum_{n=2}^{M-1} \left\| P_h^{n+1} - (\frac{7}{3}p_h^n - \frac{5}{3}p_h^{n-1} + \frac{1}{3}p_h^{n-2} - \gamma \nabla \cdot \boldsymbol{u}_h^{n+1})\right\|^2\right)^{1/2} \\ &\qquad \le C C_P \gamma^{-1} \nu^{-1/2} \max(C_* \nu^{-1/2}, \Delta t^{-1/2}, C_*, \nu) \max(\Delta t^{-1}, C_* \nu^{-1/2}), \end{aligned} \tag{4.6}$$

where $C > 0$ is independent of the timestep Δt, meshwidth h and stabilization parameter γ.

Remark 4.5. *On a fixed discretization, Theorem 3.4 proves first order convergence of grad-div stabilized BDF2Proj's boundary-condition-satisfying-velocity and modified pressure solutions to the BDF2Coupled velocity and pressure solutions, respectively, as $\gamma \to \infty$.*

Remark 4.6. *Similar to the first order case, Theorem 4.4 indicates a potential negative influence from a reduction of Δt, particularly for the pressure convergence, but since the pressure of the methods are known to converge, this effect will be reduced by the C_P term. Moreover, for most practical problems of interest, ν is small and C_* is large, making $\max(\Delta t^{-1}, C_* \nu^{-1/2})$ essentially independent of Δt in practice.*

Proof. This proof follows similar arguments as the first order case. Again we denote $\boldsymbol{e}^n := \boldsymbol{v}_h^n - \boldsymbol{u}_h^n$, and orthogonally decompose $\boldsymbol{e}^n$ by $\boldsymbol{e}^n = \boldsymbol{e}_0^n + \boldsymbol{e}_R^n$, where $\boldsymbol{e}_0^n \in \boldsymbol{V}_h$ and $\boldsymbol{e}_R^n \in \boldsymbol{R}_h$. Subtracting (4.3) from (4.4a) gives

$$\frac{1}{2\Delta t}(3\boldsymbol{e}^{n+1} - 4\boldsymbol{e}^n + \boldsymbol{e}^{n-1}, \boldsymbol{\chi}_h) - \left(P_h^{n+1} - \left(\frac{7}{3}p_h^n - \frac{5}{3}p_h^{n-1} + \frac{1}{3}p_h^{n-2}\right), \nabla \cdot \boldsymbol{\chi}_h\right) + b^*(2\boldsymbol{u}_h^n - \boldsymbol{u}_h^{n-1}, \boldsymbol{e}^{n+1}, \boldsymbol{\chi}_h)$$
$$+ b^*(2\boldsymbol{e}^n - \boldsymbol{e}^{n-1}, \boldsymbol{v}_h^{n+1}, \boldsymbol{\chi}_h) + \nu(\nabla \boldsymbol{e}^{n+1}, \nabla \boldsymbol{\chi}_h) + \gamma(\nabla \cdot e_R^{n+1}, \nabla \cdot \boldsymbol{\chi}_h) = 0 \quad (4.7)$$

for all $\boldsymbol{\chi}_h \in \boldsymbol{X}_h$. Next, choose $\boldsymbol{\chi}_h = \boldsymbol{e}^{n+1}$, which vanishes the first nonlinear term, and using the identity

$$a(3a - 4b + c) = \frac{1}{2}(a^2 + (2a - b)^2) - \frac{1}{2}(b^2 + (2b - c)^2) + \frac{1}{2}(a - 2b + c)^2,$$

we find that

$$\frac{1}{4\Delta t}\left(\left\|\boldsymbol{e}^{n+1}\right\|^2 - \left\|\boldsymbol{e}^n\right\|^2\right) + \frac{1}{4\Delta t}\left(\left\|2\boldsymbol{e}^{n+1} - \boldsymbol{e}^n\right\|^2 - \left\|2\boldsymbol{e}^n - \boldsymbol{e}^{n-1}\right\|^2\right) + \frac{1}{4\Delta t}\left\|\boldsymbol{e}^{n+1} - 2\boldsymbol{e}^n + \boldsymbol{e}^{n-1}\right\|^2$$
$$+\nu\left\|\nabla \boldsymbol{e}^{n+1}\right\|^2 + \gamma\left\|\nabla \cdot \boldsymbol{e}_R^{n+1}\right\|^2 \leq (P_h^{n+1} - \left(\frac{7}{3}p_h^n - \frac{5}{3}p_h^{n-1} + \frac{1}{3}p_h^{n-2}\right), \nabla \cdot \boldsymbol{e}_R^{n+1}) - b^*(2\boldsymbol{e}^n - \boldsymbol{e}^{n-1}, \boldsymbol{v}_h^{n+1}, \boldsymbol{e}^{n+1}).$$

The right hand side terms are majorized similar to the first order case, and we get

$$(P_h^{n+1} - \left(\frac{7}{3}p_h^n - \frac{5}{3}p_h^{n-1} + \frac{1}{3}p_h^{n-2}\right), \nabla \cdot \boldsymbol{e}_R^{n+1}) \leq \gamma^{-1}\|P_h^{n+1} - \left(\frac{7}{3}p_h^n - \frac{5}{3}p_h^{n-1} + \frac{1}{3}p_h^{n-2}\right)\|^2 + \frac{\gamma}{4}\|\nabla \cdot \boldsymbol{e}_R^{n+1}\|^2,$$

$$|b^*(2\boldsymbol{e}^n - \boldsymbol{e}^{n-1}, v_h^{n+1}, \boldsymbol{e}^{n+1})| \quad \leq \quad \frac{\nu}{2}\|\nabla \boldsymbol{e}^{n+1}\|^2 + C\nu^{-1}\|\boldsymbol{e}^n\|^2 + C\nu^{-1}\left\|\boldsymbol{e}^{n-1}\right\|^2.$$

Combining these estimates and summing over timesteps yields

$$\left\|\boldsymbol{e}^M\right\|^2 + \left\|2\boldsymbol{e}^M - \boldsymbol{e}^{M-1}\right\|^2 + \sum_{n=2}^{M-1}\left\|\boldsymbol{e}^{n+1} - 2\boldsymbol{e}^n + \boldsymbol{e}^{n-1}\right\|^2 + 2\nu\Delta t\sum_{n=2}^{M-1}\left\|\nabla \boldsymbol{e}^{n+1}\right\|^2 + 2\gamma\Delta t\sum_{n=2}^{M-1}\left\|\nabla \cdot e_R^{n+1}\right\|^2$$
$$\leq C\nu^{-1}\Delta t\sum_{n=2}^{M-1}\|\boldsymbol{e}^n\|^2 + 4\gamma^{-1}\Delta t\sum_{n=2}^{M-1}\left\|P_h^{n+1} - \left(\frac{7}{3}p_h^n - \frac{5}{3}p_h^{n-1} + \frac{1}{3}p_h^{n-2}\right)\right\|^2.$$

Applying Lemma 2.2, then reducing, gives for all $\Delta t > 0$,

$$\left\|\boldsymbol{e}^M\right\|^2 + \gamma\Delta t\sum_{n=2}^{M-1}\left\|\nabla \cdot e_R^{n+1}\right\|^2 \leq C\exp\left(\nu^{-1}\right)\gamma^{-1}\Delta t\sum_{n=2}^{M-1}\left\|P_h^{n+1} - \left(\frac{7}{3}p_h^n - \frac{5}{3}p_h^{n-1} + \frac{1}{3}p_h^{n-2}\right)\right\|^2.$$

where C can be considered independent of h and Δt. Thus we now have that

$$\left\|e^M\right\| \leq CC_P^{1/2}\gamma^{-1/2},$$

and using Lemma 2.1,

$$\Delta t \sum_{n=2}^{M} \|\nabla \boldsymbol{e}_R^n\|^2 \leq C C_P \gamma^{-2}. \tag{4.8}$$

We have left to bound $\Delta t \sum_{n=1}^{M} \|\nabla e_0^n\|^2$ to complete the velocity estimate. Choose $\chi = e_0^{n+1}$ in (4.7), which yields

$$\frac{1}{2\Delta t}\left(3\boldsymbol{e}^{n+1} - 4\boldsymbol{e}^n + \boldsymbol{e}^{n-1}, \boldsymbol{e}_0^{n+1}\right) + \nu\|\nabla \boldsymbol{e}_0^{n+1}\|^2 \\ = -b^*(2\boldsymbol{e}^n - \boldsymbol{e}^{n-1}, \boldsymbol{v}_h^{n+1}, \boldsymbol{e}_0^{n+1}) - b^*(2\boldsymbol{u}_h^n - \boldsymbol{u}_h^{n-1}, \boldsymbol{e}_R^{n+1}, \boldsymbol{e}_0^{n+1}). \tag{4.9}$$

The nonlinear terms are bounded similar to the first order case, using that the schemes converge and the smoothness assumptions of the true solution, which provides the bounds

$$\begin{aligned} b^*(2\boldsymbol{e}^n - \boldsymbol{e}^{n-1}, \boldsymbol{v}_h^{n+1}, \boldsymbol{e}_0^{n+1}) &\leq \frac{\nu}{4}\|\nabla \boldsymbol{e}_0^{n+1}\|^2 + C_*^2\nu^{-1}\|2\boldsymbol{e}^n - \boldsymbol{e}^{n-1}\|^2, \\ b^*(2\boldsymbol{u}_h^n - \boldsymbol{u}_h^{n-1}, \boldsymbol{e}_R^{n+1}, \boldsymbol{e}_0^{n+1}) &\leq \frac{\nu}{2}\|\nabla \boldsymbol{e}_0^{n+1}\|^2 + C_*^2\nu^{-1}\|\nabla \cdot \boldsymbol{e}_R^{n+1}\|^2. \end{aligned}$$

We handle the time derivative term to the first order case, after adding and subtracting $\boldsymbol{e}_R^{n+1}$ to the second argument of the first term, then applying the BDF2 identity given in the first step of this proof. This gives

$$\left\|\boldsymbol{e}^M\right\|^2 + \left\|2\boldsymbol{e}^M - \boldsymbol{e}^{M-1}\right\|^2 + \sum_{n=2}^{M-1}\left\|\boldsymbol{e}^{n+1} - 2\boldsymbol{e}^n + \boldsymbol{e}^{n-1}\right\|^2 + \nu\Delta t \sum_{n=2}^{M}\|\nabla \boldsymbol{e}_0^n\|^2 \\ \leq C(\nu^{-1} + \Delta t^{-2})\Delta t \sum_{n=1}^{M}\left\|\nabla \cdot \boldsymbol{e}_R^{n+1}\right\|^2 + \Delta t\left(\sum_{n=2}^{M-1} C(\nu^{-1}+1)\left\|\boldsymbol{e}^n\right\|^2\right) + \Delta t\left\|\boldsymbol{e}^M\right\|^2.$$

Now assuming $\Delta t < 1$, we apply Lemma 2.1 to obtain

$$\nu\Delta t \sum_{n=1}^{M}\|\nabla \boldsymbol{e}_0^n\|^2 \leq C(\nu^{-1} + \Delta t^{-2})\Delta t \sum_{n=1}^{M}\left\|\nabla \cdot \boldsymbol{e}_R^{n+1}\right\|^2,$$

where C remains independent of h and Δt. Combining this estimate with (4.8) completes the proof for velocity.

For the pressure estimate, the same technique as for the first order pressure result can be applied to get the result. □

4.2 Numerical experiments for the second order schemes

We now perform numerical tests to validate the theory above. The first test will determine the convergence rates of the projection method to the coupled method as $\gamma \to \infty$, and the second test will show how the convergence proven in this paper can be exploited so that the boundary-condition-satisfying velocity of BDF2Proj can be equipped with better mass conservation and provide accurate solutions.

4.2.1 Chorin problem

For a first test problem, we choose the Chorin problem [6]. The domain is taken to be the unit square $\Omega = (0,1) \times (0,1)$, and the true NSE solution is given by

$$\begin{aligned} u_1(x,y,t) &= -\cos(n\pi x)\sin(n\pi y)e^{-2n^2\pi^2\nu t}, \\ u_2(x,y,t) &= \sin(n\pi x)\cos(n\pi y)e^{-2n^2\pi^2\nu t}, \\ p(x,y,t) &= -\frac{1}{4}(\cos(2n\pi x) + \cos(2n\pi y))e^{-2n^2\pi^2\nu t}. \end{aligned}$$

This system solves the Navier-Stokes equations with forcing $\boldsymbol{f} = \mathbf{0}$ and initial condition $\boldsymbol{u}^0 = \langle u_1(0), u_2(0) \rangle^T$.

We choose $T = 1$, $\nu = 0.1$, $n = 1$, and $\boldsymbol{X}_h = \boldsymbol{\mathcal{P}}_2 \cap \boldsymbol{X}$, $Q_h = \mathcal{P}_1 \cap Q$ on a barycenter refinement of a uniform triangular mesh (with $h = 1/64$). We compute solutions with varying γ, and nodally enforce Dirichlet boundary conditions. Since our convergence results for BDF2Proj use a 3-step lagged pressure, we compute the first 3 timesteps with BDF2Coupled, and then use the results as initial conditions for velocity and pressure in BDF2Proj.

Results are shown in Table 3, and we observe first order convergence for both velocity and pressure as $\gamma \to \infty$ as predicted by Theorem 4.4.

γ	$\|\boldsymbol{u}_h - \boldsymbol{v}_h\|_{2,1}$	rate	$\|\hat{p}_h - P_h\|_{2,0}$	rate
0	4.496e-1	-	1.851e-1	-
1	1.934e-1	0.37	7.407e-2	0.40
10	4.019e-2	0.68	1.525e-2	0.67
100	6.006e-3	0.83	2.839e-3	0.73
1e+3	6.850e-4	0.94	3.869e-4	0.87
1e+4	6.964e-5	0.99	4.030e-5	0.98

Table 3: Differences between BDF2 projection method solutions with varying γ and coupled method solutions for the Chorin problem with h=1/16 and varying γ. In the tables, the pressure for BDF2Proj is the modified pressure $\hat{p}_h^n = \frac{7}{3}p_h^{n-1} - \frac{5}{3}p_h^{n-1} + \frac{1}{3}p_h^{n-3} - \gamma\nabla \cdot \boldsymbol{u}_h^n$.

4.2.2 3D lid driven cavity

Our final experiment is for the 3D lid driven cavity with Reynolds number Re=100. Here, we test the ability of BDF2Proj, with varying γ, to find the correct steady state solution. The domain for this problem is the unit cube, equipped with homogeneous Dirichlet boundary conditions for the velocity on all walls except on the top ($z = 1$), where $\boldsymbol{u}_{\text{lid}} = \langle 1, 0, 0 \rangle^T$. The kinematic viscosity is set to $\nu = 0.01$, which gives Reynolds number $Re = 100$. Midsliceplanes of the resolved solution are shown in Figure 3, and we note these match those found in the literature very well [24].

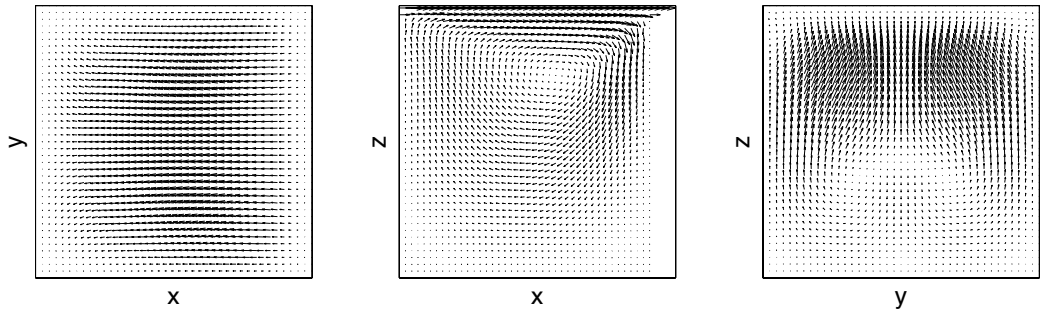

Figure 3: Shown above are the resolved midsliceplanes of the Re=100 3D driven cavity solution.

We tested BDF2Proj using $((P_3)^3, P_2^{disc})$ velocity and pressure elements on a barycenter refinement of a uniform tetrahedralization of the domain, which provided 359,373 velocity degrees of freedom and 240,000 pressure degrees of freedom. The timestep was taken to be $\Delta t = 1.0$, and the tests were run until convergence to a steady state (which we define here to be once $\|\boldsymbol{u}_h^{n+1} - \boldsymbol{u}_h^n\| < 1e-5$ is achieved).

We ran BDF2Proj using γ=0 (i.e. the standard BDF2 pressure-correction projection method), and found that it converges to an incorrect solution, shown in Figures 4 and 5. In Figure 4, we observe that the

centerline x-velocity is far from the reference values given by Wong and Baker in [24]. In Figure 5, we observe the midsliceplanes do not match the reference midsliceplanes from Figure 3 at all. It is not surprising that BDF2Proj, with $\gamma = 0$, gives a bad solution: inherent in all projection methods is a Δt dependent splitting error, and since $\Delta t = 1$, this error is substantial despite being on a relatively fine mesh for this problem.

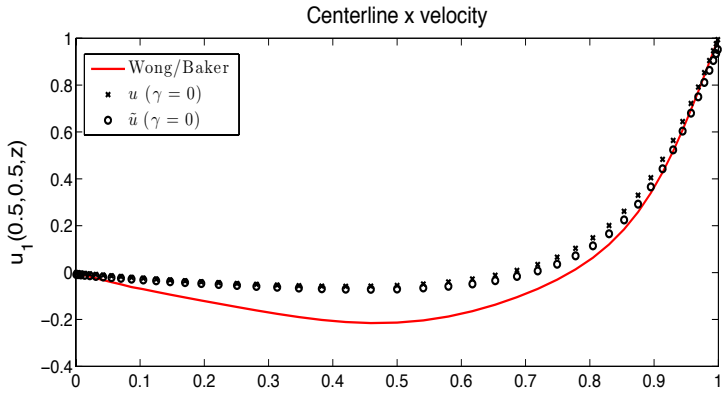

Figure 4: Shown above are the centerline x-velocities for the for the T=∞ (converged to steady state) solutions for BFDProj with γ=0.

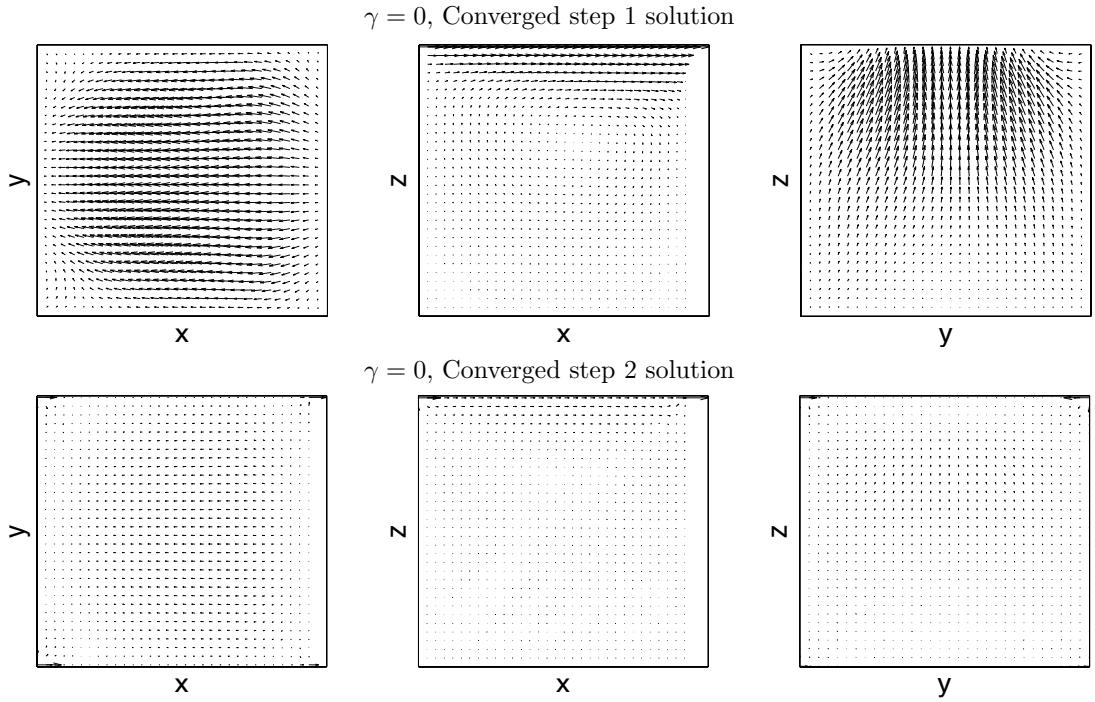

Figure 5: Shown above are the midsliceplanes for the T=∞ (converged to steady state) solutions for BFDProj with γ=0 step 1 (top) and step 2 (bottom).

Next, we ran BDF2Proj using γ=1, and saw a dramatic improvement in the steady state solution the

scheme converged to. The centerline x-velocity is shown in Figure 6 (top), and shows better agreement with the reference data of [24] compared to the γ=0 solution. The midsliceplane plots are shown in Figure 7, and the step 1 solution agrees well with the reference solution, while the step 2 solution gets larger values near the top corners.

Finally, we ran BDF2Proj using γ=10,000, and observe essentially the correct solution. The centerline x-velocity is shown in Figure 6 (bottom), and shows excellent agreement with the reference data. The midsliceplane plots are shown in Figure 7, and both the step 1 and step 2 solutions agree well with the reference solution.

We also computed divergences of the step 1 solutions (due to the element choice, step 2 solutions are all pointwise divergence-free up to the accuracy of the solver):

$$\begin{aligned} \|\nabla \cdot \boldsymbol{u}_{\gamma=0}\| &= 1.150e-0 \\ \|\nabla \cdot \boldsymbol{u}_{\gamma=1}\| &= 6.422e-2 \\ \|\nabla \cdot \boldsymbol{u}_{\gamma=10000}\| &= 7.114e-6 \end{aligned}$$

We observe that good mass conservation is provided in the γ=10,000 step 1 solution.

This example demonstrates the main point of this paper very well: the error in the projection method can be dramatically reduced by adding grad-div stabilization and using appropriate function spaces.

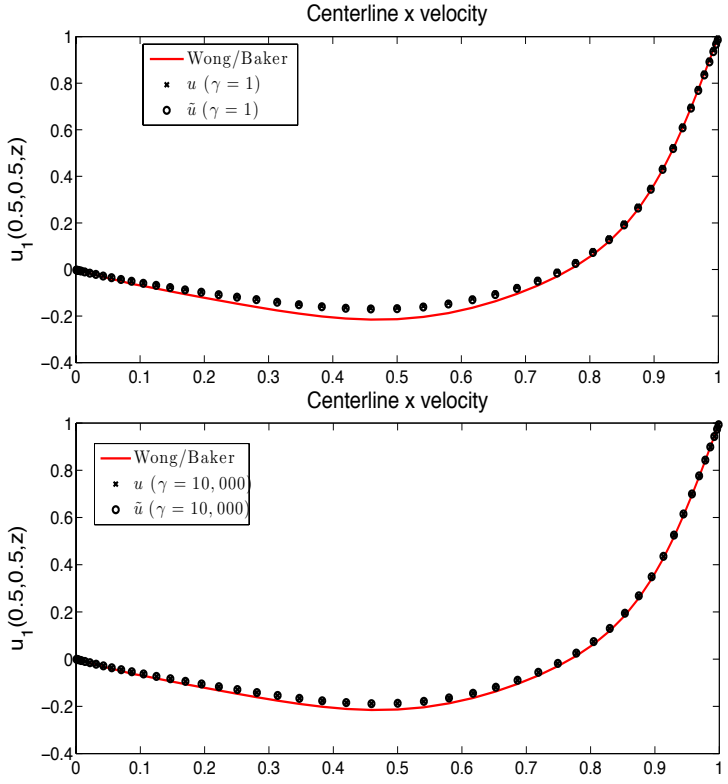

Figure 6: Shown above are the centerline x-velocities for the steady solutions of the driven cavity problem for BDF2Proj algorithm with γ=1 (top) and 10,000 (bottom).

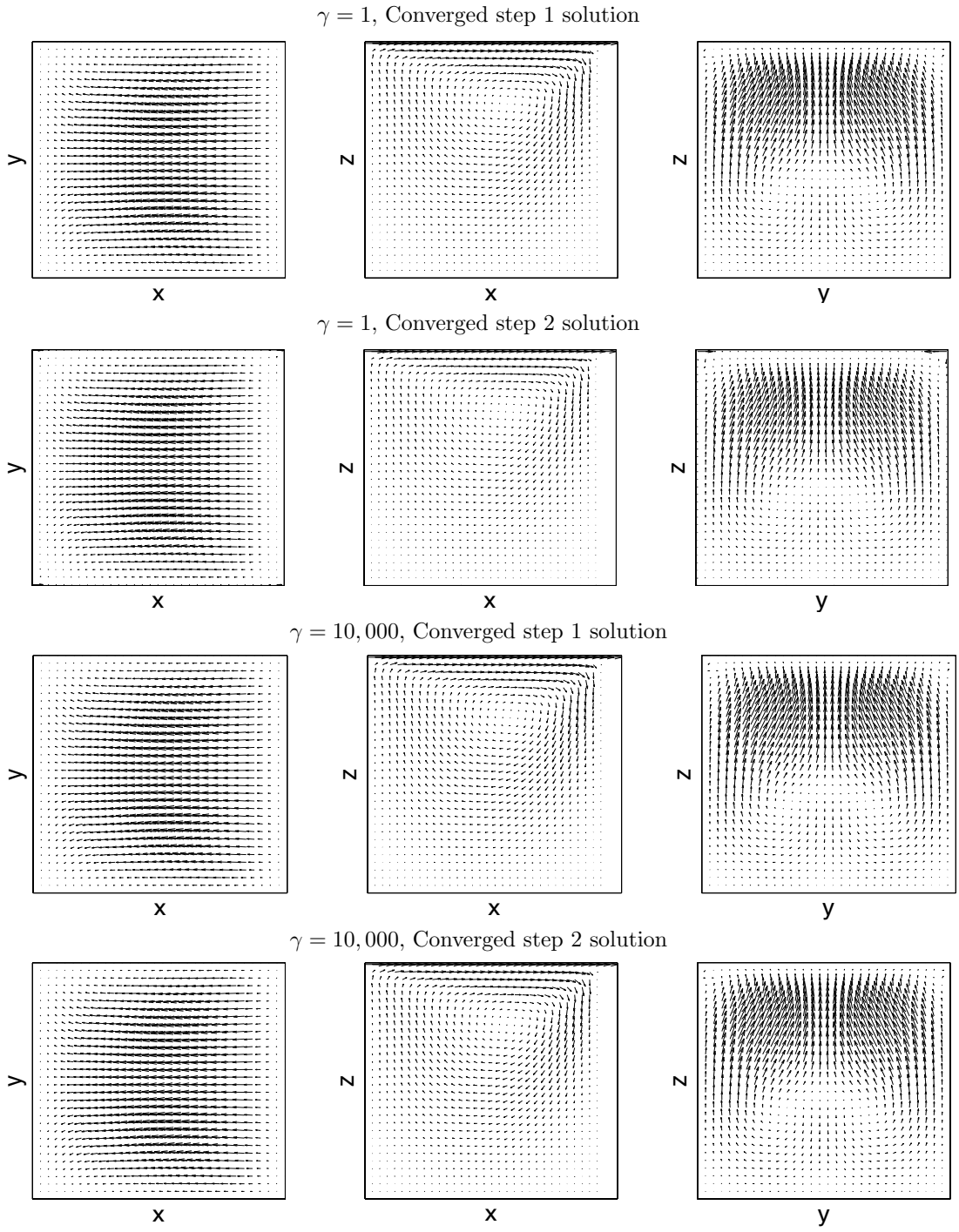

Figure 7: Shown above are the midsliceplanes for the T=∞ (converged to steady state) solutions for BFDProj with γ=1 step 1 (top) and step 2 (bottom) for γ=1 and 10,000.

5 Conclusions and discussion

We have established a strong connection between grad-div stabilized projection methods and the divergence-free coupled system method: in settings where the pointwise divergence-free subspace of the velocity space has optimal approximation properties, the grad-div stabilized solutions corresponding to the stabilization parameter $\gamma \to 0$ converge to the coupled method solution. We rigorously proved this for the 'boundary-condition-satisfying' (i.e. step 1) velocity solution of the projection method and for a modified pressure, for backward Euler and BDF2 timestepping schemes. Furthermore, Lemma 2.1 allowed us to prove the convergence was independent of h. However, both the theory and computations suggest the pressure convergence can potentially be negatively influenced by decreasing Δt, although seemingly not enough to cause any significant inaccuracy. Several numerical tests were performed to verify the theory, and show how the standard projection method can be significantly improved by using it in the way we propose.

The importance of the theory provided herein is as follows: if BDF2Proj or BELEProj is used with large grad-div stabilization in an appropriate setting (i.e. the divergence-free subspace is optimal), then the boundary-condition-satisfying solution will have good mass conservation and be very close to the corresponding BELE or BDF2 coupled scheme solution. Since it is much easier to solve the linear systems arising from projection methods compared to coupled methods, our theory makes it possible to get 'coupled-system accuracy' with 'projection-method speed'.

An important (open) related problem is how to precondition iterative methods for the linear systems arising from step 1 of BDF2Proj and BELEProj when γ is very large. Up to a few million degrees of freedom, it is shown in [7] that Matlab's backslash solver is quite effective on similar linear systems. However, for very large problems, direct solvers are no longer efficient, and one needs to use preconditioned iterative methods. To our knowledge, the only related work done near this problem is that of Schöberl in [21], in which he develops a multigrid method for linear elasticity problems when the Poisson ratio is near 0.5. This problem is exactly step 1 of BELEProj, if the time derivative and nonlinear terms are removed. Hence the authors plan to try to adapt these ideas to work with step 1 of the methods proposed herein.

A second important open problem is that of finding optimal γ for the proposed methods. Recently, in [16], this problem was considered in depth for the Stokes equations, and different dependencies on ν, h, and the true solution were found in the case when the divergence-free subspace of the velocity space has optimal approximation properties. For projection methods, the situation becomes more complicated, however, if one can determine a priori that only γ=1 or γ=10 are good choices (compared to γ=10,000), then the difficulties of linear solvers for step 1 will be significantly reduced.

References

[1] D. Arnold and J. Qin. Quadratic velocity/linear pressure Stokes elements. In R. Vichnevetsky, D. Knight, and G. Richter, editors, *Advances in Computer Methods for Partial Differential Equations VII*, pages 28–34. IMACS, 1992.

[2] M. Benzi, G. Golub, and J. Liesen. Numerical solution of saddle point problems. *Acta Numerica*, 14:1–137, 2005.

[3] M. Benzi and M. Olshanskii. An augmented Lagrangian-based approach to the Oseen problem. *SIAM J. Sci. Comput.*, 28:2095–2113, 2006.

[4] S. Brenner and L. R. Scott. *The Mathematical Theory of Finite Element Methods*. Springer-Verlag, 1994.

[5] F. Brezzi and M. Fortin. *Mixed and Hybrid Finite Elements*, volume 15 of *Springer Series in Computational Mathematics*. Springer, 1991.

[6] A. J. Chorin. Numerical solution for the Navier-Stokes equations. *Math. Comp.*, 22:745–762, 1968.

[7] B. Cousins, S. Le Borne, A. Linke, L. Rebholz, and Z. Wang. Efficient linear solvers for incompressible flow simulations using Scott-Vogelius finite elements. *Numerical Methods for Partial Differential Equations*, 29:1217–1237, 2013.

[8] H. Elman, D. Silvester, and A. Wathen. *Finite Elements and Fast Iterative Solvers with applications in incompressible fluid dynamics*. Numerical Mathematics and Scientific Computation. Oxford University Press, Oxford, 2005.

[9] Richard S. Falk and Michael Neilan. Stokes Complexes and the Construction of Stable Finite Elements with Pointwise Mass Conservation. *SIAM J. Numer. Anal.*, 51(2):1308–1326, 2013.

[10] V. Girault and P.-A. Raviart. *Finite element methods for Navier–Stokes equations: Theory and algorithms*. Springer-Verlag, 1986.

[11] J. Guermond. Un resultat de convergence d'ordre deux en temps pour l'approximation des equations de Navier-Stokes par une technique de projection incrementale. *Mathematical Modelling and Numerical Analysis*, 33(1):169–189, 1999.

[12] J. Guermond, P. Minev, and J. Shen. An overview of projection methods for incompressible flows. *Computer Methods in Applied Mechanics and Engineering*, 195:6011–6045, 2006.

[13] J.-L. Guermond. Some practical implementations of projection methods for Navier-Stokes equations. *M2AN*, 30:637–667, 1996.

[14] J. Guzmán and M. Neilan. Conforming and divergence-free stokes elements on general triangulations. *Math. Comp.*, 2013. to appear.

[15] J. Heywood and R. Rannacher. Finite element approximation of the nonstationary Navier-Stokes problem. Part IV: Error analysis for the second order time discretization. *SIAM J. Numer. Anal.*, 2:353–384, 1990.

[16] E. Jenkins, V. John, A. Linke, and L. Rebholz. On the parameter choice in grad-div stabilization for the stokes equations. *Advances in Computational Mathematics*, to appear, 2013.

[17] W. Layton. *An Introduction to the Numerical Analysis of Viscous Incompressible Flows*. SIAM, Philadelphia, 2008.

[18] W. Layton, C. Manica, M. Neda, and L. Rebholz. Numerical analysis and computational testing of a high accuracy Leray-deconvolution model of turbulence. *Numerical Methods for Partial Differential Equations*, 24(2):555–582, 2008.

[19] A. Prohl. *Projection and quasi-compressibility methods for solving the incompressible Navier-Stokes equations*. Teubner-Verlag, Stuttgart, 1997.

[20] A. Prohl. On pressure approximation via projection methods for nonstationary incompressible Navier-Stokes equations. *SIAM Journal on Numerical Analysis*, 47(1):158–180, 2008.

[21] J. Schöberl. Robust multigrid methods for a parameter dependent problem in primal variables. *Numerische Mathematik*, 84:97–119, 1999.

[22] L. R. Scott and M. Vogelius. Norm estimates for a maximal right inverse of the divergence operator in spaces of piecewise polynomials. *Mathematical Modeling and Numerical Analysis*, 19(1):111–143, 1985.

[23] R. Temam. Sur l'approximation de la solution des equations de Navier-Stokes par la methode des pas fractionnaires (II). *Arch. Rational Mech. Anal.*, 33:377–385, 1969.

[24] K.L. Wong and A.J. Baker. A 3d incompressible Navier-Stokes velocity-vorticity weak form finite element algorithm. *International Journal for Numerical Methods in Fluids*, 38:99–123, 2002.

[25] S. Zhang. A new family of stable mixed finite elements for the 3d Stokes equations. *Math. Comp.*, 74(250):543–554, 2005.